Smooth On-line Path Planning for Needle Steering with Non-linear Constraints

Christopher Burrows[1], Fangde Liu[1] and Ferdinando Rodriguez y Baena[1]

***Abstract*— Percutaneous intervention is a commonly used surgical procedure for many diagnostic and therapeutic operations. Target motion in soft tissue during an intervention caused by tissue deformation is a common problem, along with needle displacement. In this work, we present a deformation planner that generates continuous curvature paths with a bounded curvature derivative that can be used on-line to reach a moving target. This planner is computationally inexpensive and can be used for any robotic system, which has finite angular velocity, to reach a mobile target. The deformation planner, is integrated into a needle steering system using a novel, biologically inspired needle, STING, to track a simulated moving target. In-vitro results in gelatin demonstrate accurate 2D tracking of a moving target (mean 0.27 mm end positional error and 0.80° approach angle error) over 3 target movement rates.**

I. Introduction

Needle steering technology is a growing research topic within minimally invasive surgery, in particular for percutaneous intervention therapies. Further development of this technology has the potential to bring several advantages to the patient with few drawbacks.

The main principle behind needle steering is that, rather than performing a straight line path to a target region, with a straight rigid needle, a curvilinear path is performed using a flexible needle. A curvilinear path makes it possible for therapies to be applied to scenarios which may have never been possible otherwise with a straight line path, without causing excess trauma to the patient, such as multi targeting and the targeting of dynamic targets which drift away from a predefined location due to tissue deformation.

Several needle steering technologies have been developed in order to provide curvilinear paths within tissue. These can be broadly classified into 4 main categories: needle steering controlled using concentric tubes [1, 2], needle steering controlled using the lateral motion of the needle base [3] flexible needle steering controlled using a fixed shape bevel tip [4, 5] and flexible needle steering controlled using a bio-inspired multi-segment needle [6].

The latter is our attempt to tackle some of the problems with current needle steering systems. The **S**oft **T**issue **I**ntervention and **N**eurosurgical **G**uide (STING) has a unique actuation mechanism and utilises a 'programmable bevel' [7] in order to steer along arbitrary curvilinear paths. Previously, a miniaturised version of the needle, with a 4mm outside diameter (OD), coupled with a smooth path planner [6], has been shown to produce good 2D tracking results, 0.1 mm tracking error with a 0.64 mm standard deviation (SD). Further development of this needle steering system to track a moving target, with on-line path planning, on a plane is carried out in this work.

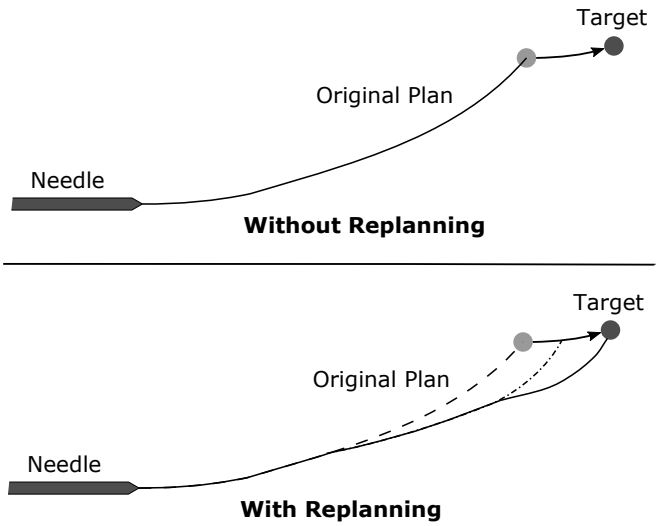


Fig. 1. **Top Diagram** - During needle insertion a target can move due to tissue deformation causing therapy to be less effective as the needle is displaced from the target. **Bottom Diagram** - With on-line replanning, the needle can be guided to the target as it moves, resulting in a more effective therapy.

Tracking of moving targets in robotics is a well researched problem. Typically it is solved with sophisticated prediction models or high frequency control systems. However, in surgical procedures, this is not always possible, as tissue deformation of non-isotropic tissue is very difficult to model and quick dynamics in a procedure would cause excess trauma. Therefore if a target moves or the location of the needle changes because of patient movement or tissue deformation, the original pre-operative plan through the tissue needs modifying. This can be achieved by on-line replanning during a procedure, as shown in Fig. 1.

Robotic non-holonomic systems that have a finite orientation velocity, e.g. car-like robots, still remain a challenge for path planning. As a consequence of these kinematics, the paths have to be smooth and have a bounded curvature derivative. Typical path planners for these systems either produce sub-optimal paths [8] or are computationally expensive [9] and therefore cannot be used on-line. In this work we present an on-line path planner that provides an optimal, shortest path, which is computationally inexpensive.

*This work was supported by the European Research Council under the European Union's Seventh Framework Programme (FP7/2007-2013) / ERC grant agreement no [258642-STING]

[1]All of the authors are from the Mechatronics in Medicine Laboratory, Mechanical Engineering Department, Imperial College London, London, UK f.rodriguez@imperial.ac.uk

Research on the control and planning of steerable needles generally ignores the complex interactions between the needle and the tissue, simplifying the kinematics by adopting the approach used to model non-holonomic vehicles [10, 11]. Even so, planning remains challenging for non-holonomic motion [12], especially with steerable needles, as the input has to be bounded. Rapidly Exploring Random Tree methods (RRT), where trajectories are made up of constant curvature segments, are the most popular in practice. However, generally in practice there is a lack of control in orientation, residual position errors and curvature discontinuities, due to the increased state size and computational expense, making the resulting paths not strictly feasible [13].

There have been attempts in the literature to produce needle steering planners that act on-line during a procedure to correct for needle positioning errors. Patil et al. [14] demonstrated a RRT based planner for rapid replanning and controlling a needle in 3D. However, this planner still suffers from the inherent RRT based problems, as well as requiring expensive hardware to operate. Duindam et al. [13] presented a fast path planner based on the inverse kinematics of a steerable needle. This path planner also generates discontinuous curvature paths and does not guarantee to produce optimal paths.

Previously Ko and Rodriguez y Baena [6] presented an iterative based gradient approach for producing smooth paths, where the curvature gradient is bounded. However, this method is computationally expensive and thus not applicable for on-line path re-planning, requiring 1000s of iterations to converge to a solution. This type of planner is therefore only suitable for initial plans of complex scenarios in pre-surgery, where many risk factors have to be considered.

In this work we present an on-line path planner based on the 'Deformation-as-Control' (DAC) planner presented in [15]. The DAC planner only considered the maximum curvature constraint for needle steering path planning. In this paper we extend the analysis presented in [15] to consider a bounded curvature derivative, which we refer to as the deformation planner. This results in a non-linear formulation of the DAC planner which we then present a computationally inexpensive linear iterative solution for. We then demonstrate the performance of the deformation planner with in-vitro trials using the STING needle steering system to track a simulated moving target.

The rest of the paper is structured as follows: Section II presents the deformation planner, Section III provides an overview of the system, then Sections IV and V present the experimental setup used to test the deformation planner and the results from these tests, respectively. Finally, Section VI presents conclusions and future work.

II. Deformation Planner Theory

The STING needle is a robotic system that requires a path constraint on the gradient of the curvature in order for it to be feasible. Ko and Rodriguez y Baena [6] previously defined the required path planning constraints for the STING needle as follows:

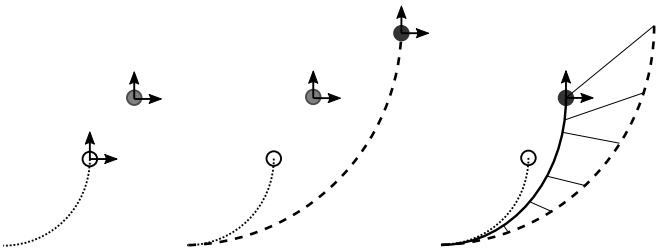


Fig. 2. Illustration of the deformation planner process. **Left**: The original path c (dots) with the original target (white) and the displaced target (light grey). **Middle**: c is deformed into a circular arc (dashed) such that the end point (dark grey) is orientated with the displaced target orientation. **Right**: The circular arc is then scaled into the final path (solid). The lines between the circular arc and final path are between equivalent points on the paths.

1) The maximum curvature of the overall path should be bounded, since the curvature is related to the offset between the two segments of the flexible needle and an excessive offset between steering segments may cause the leading one to buckle [7].
2) The maximum rate of change of the curvature should be bounded. Our feedback controller restricts the maximum speed of each segment to prevent damage to the surrounding tissue. This requirement results in a restriction to the maximum rate of change of steering offset, which in turn results in a restriction to the maximum rate of change of the path's curvature.

A. Overview of Deformation-as-Control

Previously, Liu et al. [15] presented the Deformation-as-Control (DAC) planner which transforms the complex kinematic constraints for a needle steering system into a linear formulation. In the DAC planner framework, a deformation is found that correctly deforms a circular arc to the desired target under a curvature constraint. As shown in Fig. 2, this process involves two steps:

1) The orientation of the path, $\theta(t)$, is adjusted by deforming the current path, c, into a circular arc where the end orientation is the same as the approach angle required at the target
2) A scaling function, $s(t)$, is then applied over the arc so that the resultant path matches the required start and end positions, with the required curvature constraints.

To solve this problem numerically, the path is split into n segments, where the start and end points and curvature constraints then become linear. Since the shortest path through the tissue is desirable to reduce overall trauma, the following linear optimization problem is then solved to minimise the overall path length, L:

$$\begin{aligned} \text{minimize:} \quad & L(s) \\ \text{subject to:} \quad & A(\theta)s = [x, y] \\ & s > \frac{1}{k_{max}} \end{aligned} \tag{1}$$

Where θ and s are the orientation and scaling functions respectively and k_{max} is the maximum allowable curvature.

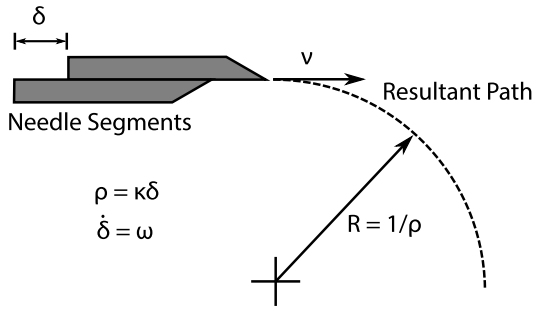


Fig. 3. STING needle kinematics. An offset between the needle's segments, δ, when pushed into tissue with constant velocity, ν, causes the needle to take a constant curvature, ρ, path through the tissue. The relationship between base offset and resultant curvature has been shown to be linear represented by a constant, κ. See Burrows et al. [16] and Ko and Rodriguez y Baena [7] for more details.

Derivations of matrices A and L can be found in the appendix of [15].

B. Derivative of Curvature

The maximum derivative of curvature, $\dot{\rho}$, for the STING needle can be calculated from the ratio of the rate of change of the steering offset, $\dot{\delta} = \omega$, and forward velocity, ν, and the steering constant (see Fig. 3), κ:

$$\dot{\rho} = \kappa \frac{\omega}{\nu} \tag{2}$$

For the controller used in this work, the maximum ω is constrained to be twice ν, so the segments do not move backwards at any point. The maximum rate of change of curvature then becomes:

$$max(\dot{\rho}) = 2\kappa \tag{3}$$

In order to add a derivative curvature constraint to the problem statement in Equation 1, the derivative of curvature has to be defined in the deformation framework. Since the curvature, k, is the inverse of the scaling function, s, the curvature derivative, k', of the path can be found in terms of s and t:

$$\begin{aligned} k' &= \frac{dk}{dL} = \frac{\frac{dk}{dt}}{\frac{dL}{dt}} \\ \frac{dk}{dt} &= \frac{d(1/s)}{dt}, \quad \frac{dL}{dt} = s \\ k' &= \frac{-1}{s^3}\frac{ds}{dt} \end{aligned} \tag{4}$$

For each of the segments along the path, s is linearly interpolated between the start and end points, s_a and s_b respectively, and thus, for each of the segments, $\frac{ds}{dt} = \frac{s_b - s_a}{t_d}$ is fixed and thus:

$$k' = \frac{s_a - s_b}{t_d s^3} \quad \text{for } s \text{ in } [s_a, s_b] \tag{5}$$

where t_d is the difference of parameter t at points a and b. As can be seen in Equation 5, the maximum curvature gradient occurs at either the start or end points. Therefore the curvature derivative constraint becomes:

$$k'_{max} > \max\left(\left|\frac{s_a - s_b}{t_d s_a^3}\right|, \left|\frac{s_a - s_b}{t_d s_b^3}\right|\right) \tag{6}$$

Equation 6 is non-linear and at this point could be added to the formulation in Equation 1 and solved with a general non-linear optimizer. However, this approach would be computationally expensive, therefore an alternative solution is presented in the following sections.

C. Relaxation of the Constraints and Numerical Techniques

Instead of using a generalized non-linear optimization method for solving Equations 1 and 6, an alternative, efficient numerical method is developed from the unique structure of our problem. First, the constraints are relaxed and rewritten in the linear form:

$$k'_{max} t_d B^3 > |s_a - s_b| \tag{7}$$

Where $B = \max(s_a, s_b)$. Here B represents a conservative guess for the lower boundary of $[s_a, s_b]$.

It can then be shown that a solution to Equations 1 and 6 must satisfy Equations 1 and 7. To tighten these constraints and thus iteratively converge to a solution that satisfies Equation 6, the following iteration can then be used:

$$B_{i+1} = \max(s_{ia}, s_{ib}) \tag{8}$$

where s_{ia} and s_{ib} are computed by solving Equations 1 and 7 directly. The iterative process continues until B_i satisfies Equation 6. As most numerical optimisation packages are iterative solvers, the speed of convergence depends heavily on the quality of the starting points. As this method updates the constraints during the iteration process, the convergence to a solution is fast as the starting points are close to the solution.

D. Initial Guess

To produce an initial guess, B_0, for the iterative process in Equation 8, the constraints in Equations 1 and 7 are solved. The resultant points then define a convex hull of the optimisation workspace where each of the vertices describes a valid path. This convex hull defines all of the feasible path workspace, thus estimating the centroid of the vertices will provide a good initial guess for the iterative process.

III. Control

This section provides an overview of how the controller and deformation planner interact in the system.

As can be seen in Fig. 4, the process is broken into two processes, the Initial Phase and the Control Phase. The Initial Phase is for the initial calibration of the experimental setup and generation of the initial path (surgical plan) between the insertion point and the target. The Control Phase contains the components of the system that are used to guide the needle to the moving target in a deformable environment. Sections III-A and III-B explain each of these phases in detail.

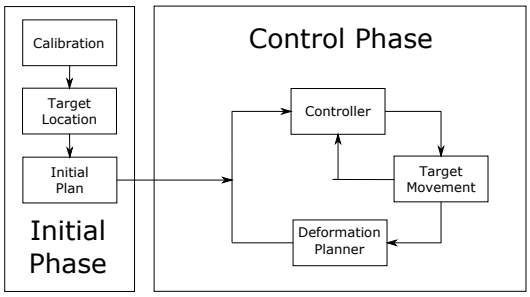


Fig. 4. Overview of how the needle steering system operates - separated into two processes, the initial phase and control sequence respectively.

A. Initial Phase

In Fig. 4 there are 3 different processes in the Initial Phase, Calibration, Target Location and Initial Planner. The Calibration process determines the insertion plane and the origin of the control coordinate frame and registers the needle in the global workspace. The Target Location process then determines the location of the target in the control coordinate frame. For this work, the target is simulated and moves according to the description in Section IV-A. The Initial Plan process, using a suitable pre-operative path planner, then determines a trajectory to the target, considering the surgical environment and constraints. For this work, we used the path planner from [6], as it considers the curvature derivative constraint required for the STING needle.

B. Control Sequence

Once an initial path is set, the control sequence in charge of driving the needle to a target is started, as shown in Fig. 4.

The following steps are then iterated:

Step 1 Given the current path, the controller guides the needle along this path.

Step 2 After a set time period, t_m, the location of the target is observed. If the target has been displaced above a threshold, D_{max}, move to Step 3, otherwise move to Step 1 (this step is represented by the central arrow in Fig. 4).

Step 3 The deformation planner is used to generate a new path based on the current state of the needle, new location of the target and required approach angle. Move to Step 1.

The Control Phase is repeated until the target has been reached.

IV. Experimental Setup

A. Target Movement and Location

To test the performance of the planner, a simulated moving target was used. Three movement rates, shown in Table I, were considered to demonstrate the ability of the system to reach the target over a variety of displacements magnitudes. These rates were chosen such that the total displacement of the target approximately matches that found in soft tissue procedures [17, 18, 19].

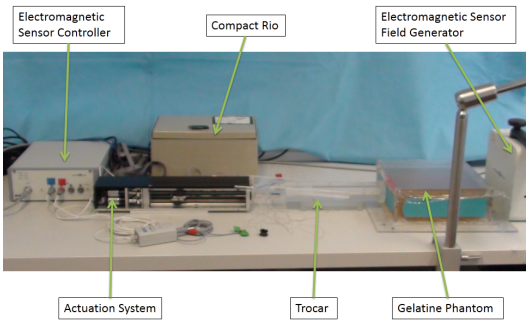


Fig. 5. Picture of the experimental setup used to test the deformation planner.

The direction of the movement of the target is controlled in two primary directions. Firstly, the target moves at a constant rate (values in Table I) along the starting needle insertion axis. Then, when the needle is close enough to the target ($\leq$20mm), the target also moves with a rate of 0.075 mm/s, average displacement rate seen in [20], in the direction of the needle axis. This simulates the type of deformation seen from inserting the needle into soft tissue, as shown in [20]. The two movement vectors are summed when both are operating.

For all experiments, the starting target location is at (125, 25), with an approach angle of 32.3°. The initial plan and therefore the approach angle was generated using the planner from [6].

TABLE I. Simulated Movement Rates

Name	Movement Rate (mm/s)	Approx. Total Displacement (mm)
Small	0.015	3.0
Medium	0.025	5.0
Large	0.05	10.0

B. Setup

Fig. 5 shows the experimental setup used to control the needle steering system. The actuation box is the same as that used previously [7, 6], where a set of linear actuators are controlled via a CompactRIO controller (National Instruments Corp.) [21]. The controller from [7] and the deformation controller were implemented in a custom C++ and python program. An Electromagnetic (EM) tracking sensor (Aurora 5 DOF sensor with 0.55 mm diameter and 8 mm length, Northern Digital Inc. [22]), with a root-mean square (RMS) accuracy of 0.9 mm, was attached to one of the segments to measure the needles tip position throughout the experiments. Bovine gelatin, 250 bloom (Sleaford Quality Foods, Sleaford, UK), 4.5 wt% was used as the tissue phantom in the experiments. This gelatine was shown in preliminary tests to have a similar Young's Modulus, 7 kPa, to the gelatine used in previous work [6]. The parameters, determined empirically, used for the controller and planners are shown in Table II. Each of the experiments was performed three times with

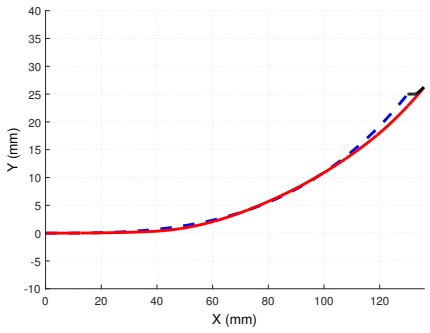


Fig. 6. Smoothed resultant needle path (red) from medium target movement experiment with initial plan (blue dashed) and target path (black).

each of the movement rates in Table I, for a total of nine experiments overall.

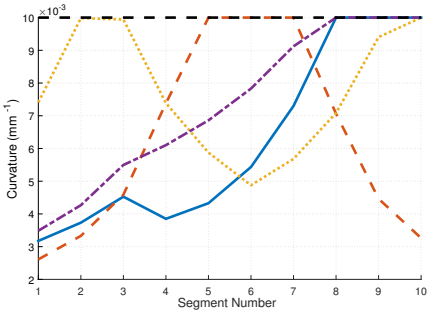
TABLE II. Experimental Parameters

Parameter	Symbol(s)	Value
Initial Plan		
Start State	$[x_0, y_0, \theta_0, k_0]$	[0,0,0,0]
Max. Curvature	k_{max}	0.01 mm^{-1}
Max. Deriv. Curvature	k'_{max}	7.80×10^{-4} mm^{-2}
Controller		
Compensation Coefficient	ϵ	2.4
Steering Coefficient	κ	3.90×10^{-4} mm^{-2}
Max. Steering Offset	δ_{max}	30 mm
Sampling Time	Tp	2 s
Subsampling Time	Ts	0.25 s
Prediction Horizon	Np	10
Subsample Prediction Horizon	Ns	8
Deformation Planner		
Number of Segments	n	10
Max. Curvature	k_{max}	0.01 mm^{-1}
Max. Deriv. Curvature	k'_{max}	7.80×10^{-4} mm^{-2}
Target Movement Threshold	D_{max}	0.2 mm

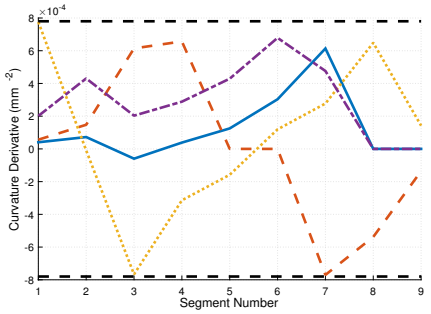
V. Results and Discussion

Fig. 6 shows the results from one of the experiments carried out with the medium target movement rate. Table III shows the mean positional and angle results for all the movement rates and the total mean positional and angular errors. Across all movement rates, the mean end positional error was 0.27mm with a SD of 0.20 and the mean approach angle error was 0.8 Rad. with a SD of 0.22. The positional errors are similar to results that been achieved previously in 2D with STING [6] and other needle steering systems [5] in 2D to a static target. The mean overall target displacement for the movement rates (small, medium, large) were 3.6 mm, 7.8 mm and 11.1 mm respectively. For all of the experiments, the average iteration time was 7 ms, with a mean of 2.7 iterations per replan. Fig. 7b shows the curvature and curvature derivative over the segments of the resultant replans from various points through the insertion. From this it can be seen that the deformation planner adheres to the required constraints.

These results demonstrate that the deformation planner, in combination with a suitable controller, can be used to guide the needle to a single moving target, across a range



(a) Curvature of Generated Plans



(b) Curvature Derivative of Generated Plans

Fig. 7. Curvature (a) and curvature derivative (b) of several generated plans by the deformation planner, during the experiment shown in Fig. 6 at different target displacements, blue - 0.6 mm , orange - 1.2 mm, yellow - 1.8 mm, purple - 2.6 mm. The dashed black lines represent the respective bounds of each variable.

of target movement rates and total displacements, with a position error which would be acceptable in most needle-based surgical procedures [19]. The rate of movement and the overall displacement of the target does not appear to affect the ability of the system to guide the needle to the target position with all the mean end position errors showing similar values and SDs. The results also show that the needle tracks the approach angle of each target very closely over all the scenarios.

The proposed planner is also quick, with a mean iteration time and number of iterations of 7 ms and 2.7 respectively and adheres to the required constraints.

TABLE III. End Position and Approach Angle Error Results

	End Position Error (mm)		Approach Angle Error (Deg.)	
Deformation	*Mean*	*SD*	*Mean*	*SD*
Small	0.24	0.10	0.80	0.17
Medium	0.32	0.29	0.69	0.11
Large	0.25	0.20	0.97	0.40
Total	0.27	0.20	0.80	0.22

VI. Conclusions and Future Work

This work describes a combined system for guiding a needle to a moving target within deforming soft tissue. A deformation planner is presented that can be used on-line to guide a needle to a single moving target. Based

on deformation theory, it is demonstrated that the non-linear constraint of a bounded curvature derivative can be formulated into a iterative linear optimisation problem. As a consequence, the deformation planner produces smooth paths, in a computationally inexpensive manner, which have a bounded curvature gradient. This planner is applicable to any robotic system where the orientation cannot be changed instantaneously, such as car-like systems.

The system was tested experimentally using a STING needle prototype in a gelatine phantom. Three experiments were carried out for each of three different target movement rates, for nine total experiments. The results showed that the system could successfully guide the needle in a 2D plane to a moving target with a total mean end position error of 0.27mm and total mean approach angle error of 0.8°.

There is significant scope for future work. Firstly, it is possible to expand the current system to scenarios where multiple targets are considered during the same insertion. It is also planned to demonstrate the deformation planner's performance in 3D scenarios.

REFERENCES

[1] P. E. Dupont, J. Lock, B. Itkowitz, and E. Butler, "Design and control of concentric-tube robots," *Robotics, IEEE Transactions on*, vol. 26, no. 2, pp. 209–225, 2010.

[2] R. J. Webster and B. A. Jones, "Design and kinematic modeling of constant curvature continuum robots: A review," *The International Journal of Robotics Research*, 2010.

[3] D. Glozman and M. Shoham, "Image-guided robotic flexible needle steering," *Robotics, IEEE Transactions on*, vol. 23, no. 3, pp. 459–467, 2007.

[4] A. Majewicz, T. R. Wedlick, K. B. Reed, and A. M. Okamura, "Evaluation of robotic needle steering in ex vivo tissue," in *Robotics and Automation (ICRA), 2010 IEEE International Conference on*. IEEE, 2010, pp. 2068–2073.

[5] V. Kallem and N. Cowan, "Image guidance of flexible tip-steerable needles," *Robotics, IEEE Transactions on*, vol. 25, no. 1, pp. 191–196, 2009.

[6] S. Y. Ko and F. Rodriguez y Baena, "Toward a miniaturized needle steering system with path planning for obstacle avoidance," *Biomedical Engineering, IEEE Transactions on*, vol. 60, no. 4, pp. 910–917, 2013.

[7] ——, "Trajectory following for a flexible probe with state/input constraints: An approach based on model predictive control," *Robotics and Autonomous Systems*, vol. 60, no. 4, pp. 509–521, 2012.

[8] E. Bakolas and P. Tsiotras, "On the generation of nearly optimal, planar paths of bounded curvature and bounded curvature gradient," in *American Control Conference, 2009. ACC '09.*, June 2009, pp. 385–390.

[9] T. G. McGee, S. Spry, and J. K. Hedrick, "Optimal path planning in a constant wind with a bounded turning rate," in *AIAA Guidance, Navigation, and Control Conference and Exhibit*. Reston, VA, 2005, pp. 1–11.

[10] R. J. Webster, J. S. Kim, N. J. Cowan, G. S. Chirikjian, and A. M. Okamura, "Nonholonomic modeling of needle steering," *The International Journal of Robotics Research*, vol. 25, no. 5-6, pp. 509–525, 2006.

[11] S. Y. Ko, L. Frasson, and F. Rodriguez y Baena, "Closed-loop planar motion control of a steerable probe with a programmable bevel inspired by nature," *Robotics, IEEE Transactions on*, vol. 27, no. 5, pp. 970–983, 2011.

[12] A. M. Bloch, *Nonholonomic mechanics and control*. Springer, 2003, vol. 24.

[13] V. Duindam, J. Xu, R. Alterovitz, S. Sastry, and K. Goldberg, "Three-dimensional motion planning algorithms for steerable needles using inverse kinematics," *The International Journal of Robotics Research*, vol. 29, no. 7, pp. 789–800, 2010.

[14] S. Patil, J. Burgner, R. Webster, and R. Alterovitz, "Needle steering in 3-d via rapid replanning," pp. 1–12, 2014.

[15] F. Liu, C. Burrows, and F. Rodriguez y Baena, "Deformation-as-control for a biologically inspired steerable needle," in *Robotics and Biomimetics (ROBIO), 2013 IEEE International Conference on*, Dec 2013, pp. 848–853.

[16] C. Burrows, R. Secoli, and F. Rodriguez y Baena, "Experimental characterisation of a biologically inspired 3d steering needle," in *Control, Automation and Systems (ICCAS), 2013 13th International Conference on*. IEEE, 2013, pp. 1252–1257.

[17] J. R. Lobo, M. Moradi, N. Chng, E. Dehghan, W. J. Morris, G. Fichtinger, and S. E. Salcudean, "Use of needle track detection to quantify the displacement of stranded seeds following prostate brachytherapy," *Medical Imaging, IEEE Transactions on*, vol. 31, no. 3, pp. 738–748, 2012.

[18] E. E. Deurloo, K. G. Gilhuijs, L. J. S. Kool, and S. H. Muller, "Displacement of breast tissue and needle deviations during stereotactic procedures," *Investigative radiology*, vol. 36, no. 6, pp. 347–353, 2001.

[19] G. Wan, Z. Wei, L. Gardi, D. B. Downey, and A. Fenster, "Brachytherapy needle deflection evaluation and correction," *Medical physics*, vol. 32, no. 4, pp. 902–909, 2005.

[20] M. Oldfield, C. Burrows, J. Kerl, L. Frasson, T. Parittotokkaporn, F. Beyrau, and F. Rodriguez y Baena, "Highly resolved strain imaging during needle insertion: Results with a novel biologically inspired device," *Journal of the mechanical behavior of biomedical materials*, vol. 30, pp. 50–60, 2014.

[21] National Instruments Corporation, "NI CompactRIO," http://www.ni.com/compactrio/, 2014, [Online; accessed Sept-2014].

[22] Northern Digital Inc., "The Aurora Electromagnetic Tracking System," http://www.ndigital.com/medical/products/aurora/, 2014, [Online; accessed Sept-2014].